ACS NANO
Cite This: ACS Nano 2018, 12, 3681−3688
www.acsnano.org

ARTICLE

Polarization Rotation in Ultrathin Ferroelectrics Tailored by Interfacial Oxygen Octahedral Coupling

Sirui Zhang,[†,‡] Xiangwei Guo,[†,§] Yunlong Tang,[†] Desheng Ma,[⊥] Yinlian Zhu,*[,†] Yujia Wang,[†] Shuang Li,[†,‡] Mengjiao Han,[†,‡] Dong Chen,[†] Jinyuan Ma,[†,‡,∥] Bo Wu,[†,§] and Xiuliang Ma*[,†,∥]

[†]Shenyang National Laboratory for Materials Science, Institute of Metal Research, Chinese Academy of Sciences, Wenhua Road 72, Shenyang 110016, China

[‡]University of Chinese Academy of Sciences, Yuquan Road 19, Beijing 100049, China

[⊥]School of Physics, Nankai University, Weijin Road 94, Tianjin 300071, China

[§]School of Materials Science and Engineering, University of Science and Technology of China, Hefei 230026, China

[∥]School of Materials Science and Engineering, Lanzhou University of Technology, Langongping Road 287, Lanzhou 730050, China

Supporting Information

ABSTRACT: **Multiple polar states and giant piezoelectric responses could be driven by polarization rotation in ferroelectric films, which have potential functionalities in modern material applications. Although theoretical calculations have predicted polarization rotation in pure $PbTiO_3$ films without domain walls and strains, direct experiment has rarely confirmed such polar states under this condition. Here, we observed that interfacial oxygen octahedral coupling (OOC) can introduce an oxygen octahedral rotation, which induces polarization rotation in single domain $PbTiO_3$ films with negligible strains. We have grown ultrathin $PbTiO_3$ films (3.2 nm) on both $SrTiO_3$ and Nb:$SrTiO_3$ substrates and applied aberration-corrected scanning transmission electron microscopy (STEM) to study the interfacial OOC effect. Atomic mappings unit cell by unit cell demonstrate that polarization rotation occurs in $PbTiO_3$ films on both substrates. The distortion of oxygen octahedra in $PbTiO_3$ is proven by annular bright-field STEM. The critical thickness for this polarization rotation is about 4 nm (10 unit cells), above which polarization rotation disappears. First-principles calculations manifest that the interfacial OOC is responsible for the polarization rotation state. These results may shed light on further understanding the polarization behavior in ultrathin ferroelectrics and be helpful to develop relevant devices as polarization rotation is known to be closely related to superior electromechanical responses.**

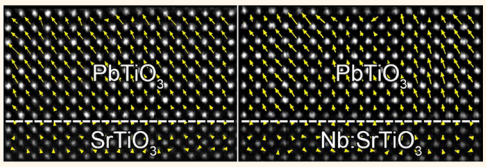

KEYWORDS: *ferroelectric material, interface coupling, ultrathin $PbTiO_3$ film, polarization rotation, aberration-corrected scanning transmission electron microscopy*

Ferroelectric films feature a multiple coupling effect which makes them technologically significant for sensors, actuators, and ultrahigh density nonvolatile memories.[1,2] In particular, multiple polar states and giant piezoelectric responses could be driven by polarization rotation in ferroelectric films,[3−6] which have potential applications as multiple state memories and high-performance piezoelectrics in commerce.[7,8] Thus, it is important to explore mechanisms that could integrate such polarization rotation in ferroelectrics with a rigid polar axis. For instance, in 5 nm thick tetragonal $PbTiO_3$ films, polarization rotation under a tensile strain was observed by synchrotron X-ray diffraction.[9] Moreover, flexoelectricity, the coupling between strain gradient and polarization, was found to generate the polarization rotation away from the tetragonal axis of 30 nm thick $PbTiO_3$ films, as observed by synchrotron X-ray diffraction and high-angle annular dark-field scanning transmission electron microscopy (HAADF-STEM).[10] In addition, the polarization rotation is the intrinsic property which would introduce giant piezoelectric response in $PbZr_{0.52}Ti_{0.48}O_3$ ferroelectrics, as verified by Noheda *et al.*[11,12]

On the other hand, the effect of the interface is an effective way for tuning or creating physical phenomena of ultrathin films,[13] such as two-dimensional electron gas,[14] magnetoelectric coupling effect,[15] and polarization enhancement.[16,17] Moreover, the coupling at the interface between tetragonal (T) $PbZr_xTi_{1-x}O_3$(PZT) and rhombohedral (R) $PbZr_xTi_{1-x}O_3$(PZT) gives rise to a polarization rotation state in both PZT films.[18] Particularly, as predicted by first-principles calculations, interface

Received: February 1, 2018
Accepted: April 9, 2018
Published: April 9, 2018

DOI: 10.1021/acsnano.8b00862
ACS Nano 2018, 12, 3681−3688

coupling may lead to the antiferrodistortive (AFD) state in the $PbTiO_3$ layer of $PbTiO_3/PbZrO_3$ superlattices,[19] where the AFD is strongly related to the oxygen octahedral rotation (OOR) in perovskite. It is also predicted that a 1/1 $PbTiO_3$/ $SrTiO_3$ superlattice results in the occurrence of the AFD state inside the oxygen octahedra of the $PbTiO_3$ layer,[20,21] where the ferroelectricity and AFD are also strongly coupled in $(PbTiO_3)_n/(SrTiO_3)_n$ superlattices by first-principles calculations.[22] However, direct experiment has rarely proven this AFD in pure $PbTiO_3$ crystals.

Furthermore, oxygen octahedral coupling (OOC) at the heterointerface is also identified for producing interesting physical phenomenon. For example, Kim *et al.* experimentally observed a nonequilibrium structure including NiO_6 octahedral tilt, which led to a polar state[23] in $NdNiO_3$ films grown on the $LaAlO_3(111)$ substrate. An oxygen octahedral proximity effect[24] at heterointerfaces due to the corner connectivity of BO_6 octahedra is also observed, which enables OOR to transfer from the substrate to the film. In addition, the OOR, induced by interfacial OOC, was found in $La_{0.7}Sr_{0.3}MnO_3$ film at the interface region, which causes changes in magnetic anisotropy.[25]

For $PbTiO_3$, first-principles calculations predicted OOR by OOC.[19−22] However, direct experiment has rarely confirmed this OOR in pure $PbTiO_3$. Here, we not only observed oxygen octahedral distortion by OOC in ultrathin $PbTiO_3$ films, but we also found that this oxygen octahedral distortion has further induced polarization rotation in these $PbTiO_3$ films. We grow epitaxial $PbTiO_3$ ultrathin films on $SrTiO_3$ and Nb:$SrTiO_3$ substrates. We found the impact of OOC on the physical features, here, the spontaneous polarization rotation state in ultrathin $PbTiO_3$ films (3.2 nm), as evidenced by aberration-corrected HAADF-STEM and annular bright field (ABF)-STEM. First-principles calculations also show that when OOR is considered, the polarization rotation states become stable. More importantly, the interface coupling is the key role to the distortion of oxygen octahedra and further generates polarization rotations in ultrathin films.

RESULTS AND DISCUSSION

Bulk $PbTiO_3$ (PTO) has a tetragonal structure with lattice parameters of $a = b = 3.904$ Å and $c = 4.157(5)$ Å (ref 26) at room temperature. $SrTiO_3$ (STO) has a cubic structure with lattice parameters of $a = 3.905$ Å, which is almost equal to the lattice parameter a of PTO. In PTO, both the Ti^{4+} ion and the oxygen octahedron have the same direction displacement from the center of the Pb lattice, where the shift of the oxygen octahedron is bigger than that of the Ti^{4+} ion, which gives rise to the spontaneous polarization along [001],[27] as shown in Figure 1. Thus, we can obtain the polarization direction in PTO films according to the shift of the Ti^{4+} ion. Figure 1a is the 3D schematic perspective view of the unit cell of PTO, which gives the atom site and oxygen octahedron in PTO. Projections of the unit cell along [100] and [1$\bar{1}$0] directions are shown in Figure 1b,c, respectively. From these sketch maps, if we want to record oxygen atoms, it is better to observe them along [1$\bar{1}$0] than along [100] as O^{2+} and Ti^{4+} overlap with each other in the [100] direction and the density of O in one O atomic column in [1$\bar{1}$0] is higher than that in [100]. Along both directions, the shift direction of Ti^{4+} can be used to determine the polarization direction and is opposite to the ferroelectric spontaneous polarization. PTO thin films about 3.2 nm thick were grown on STO(001) and Nb:STO(001) substrates, as shown in Figure 1d,e. The selection of both STO and Nb:STO substrates is to judge the influences of different screening characteristics on the

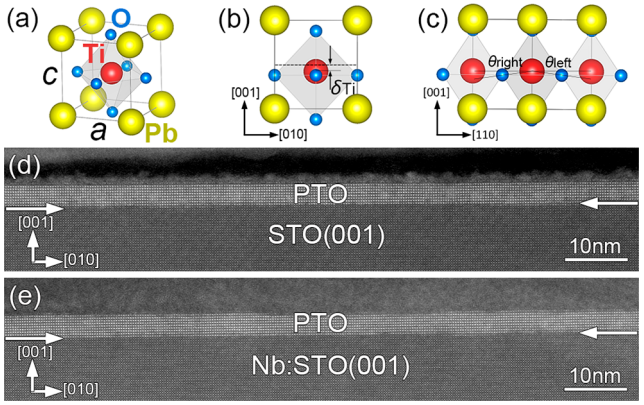

Figure 1. (a) Schematic perspective view of the unit cell of $PbTiO_3$ (yellow, Pb; red, Ti; blue, O). (b) Projection of the unit cell along the [100] direction. (c) Projection of the unit cell along the [1$\bar{1}$0] direction. (d,e) Low-magnification HAADF-STEM images along the [100] direction showing 3.2 nm thick $PbTiO_3$ layers on $SrTiO_3$ and Nb:$SrTiO_3$.

polarization behaviors of ultrathin PTO films, with one being insulating and the other being conductive. We have found that the film surfaces are extremely flat with negligible roughness, and the interfaces are also very sharp. Because the film and the substrate match very well, the present PTO/STO and PTO/Nb:STO interfaces are completely coherent without dislocations, and no domain walls were observed from the GPA results (see Supporting Information Figure S1).

A high-resolution HAADF-STEM image of the film system (PTO/STO) is shown in Figure 2a, where the PTO/STO coherent interface is marked by a pair of opposite white arrows. By means of aberration-corrected STEM,[28] we can easily obtain the atomic information on ultrathin films.[27,29,30] Lattice parameters extracted from atomic-resolution HAADF-STEM images using two-dimensional (2D) Gaussian fitting[31,32] of atomic positions are shown in Figure 2b. From Figure 2b, the in-plane lattice parameter a of the PTO films is nearly constant as STO, confirming that the PTO films are indeed uniformly strained because they have negligible strains. In contrast, the out-of-plane lattice parameter c of the PTO film increases gradually with increasing distance from the interface, reaching a maximum ($c = 4.12$ Å) at a distance of about 4 unit cells away from the interface, that is, in the middle of the film. Taking $a = 3.905$ Å, this translates to a tetragonality of $c/a \approx 1.055$. This value is somewhat smaller than the bulk value of 1.065 ($4.157/3.904 \approx 1.065$). From Figure 2b, progressing from the center of the PTO film toward the interface or the film surface, the lattice c decreases, which indicates evidently that the suppression occurs in the interfacial layer and surface in ultrathin PTO films. Figure 2c displays a superposition of the reversed δ_{Ti} vector mapping with the atomic image. Polarization directions are determined by Ti^{4+} displacements. It is found unexpectedly that the polarization rotates in PTO, which is indicated by yellow arrows. The δ_{Ti} vectors are marked by arrows located at the Ti^{4+} columns. Figure 2d gives the quantitative results for the in-plane δ_{Ti}, which is defined in the inset.

A similar analysis is performed for ultrathin PTO films on Nb:STO. A high-resolution HAADF-STEM image of the film system is shown in Figure 3a,b and gives the quantitative results. The changing trends of the lattice parameters are the same as those of the PTO film on STO. It gives the superposition of the reversed δ_{Ti} vector mapping with the atomic

DOI: 10.1021/acsnano.8b00862
ACS Nano 2018, 12, 3681−3688

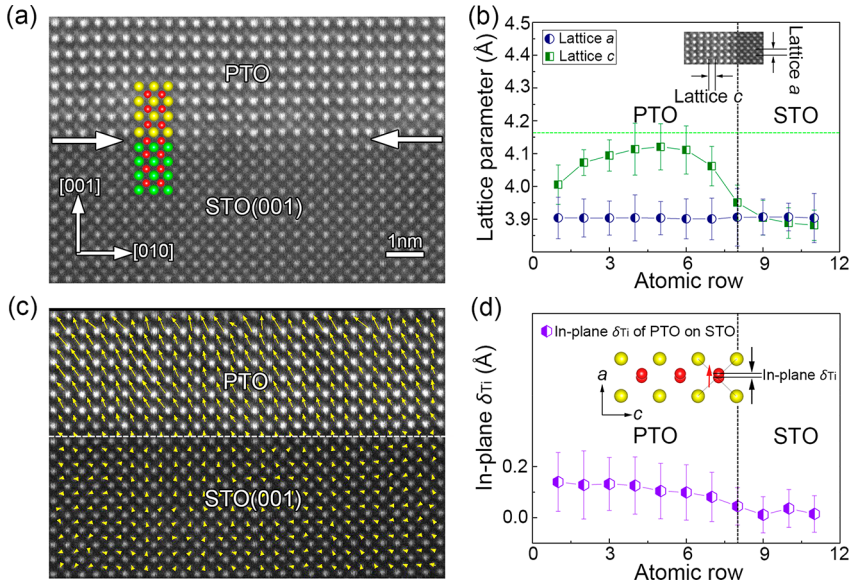

Figure 2. (a) High-magnification STEM image along the [100] direction of 3.2 nm thick $PbTiO_3$ on $SrTiO_3$. (b) In-plane and out-of-plane lattice parameter distributions of the $PbTiO_3$ films on the $SrTiO_3$. Horizontal dotted line marks the lattice parameter c of bulk tetragonal $PbTiO_3$, which is 4.157(5) Å. (c) Superposition of the reversed δ_{Ti} vectors with experimental images. The reversed δ_{Ti} vectors corresponding to $PbTiO_3$ unit cells are shown as yellow arrows superimposed on the atomic image of (a). (d) In-plane displacement of Ti^{4+} relative to Pb^{2+}, in which δ_{Ti} is defined as an inset.

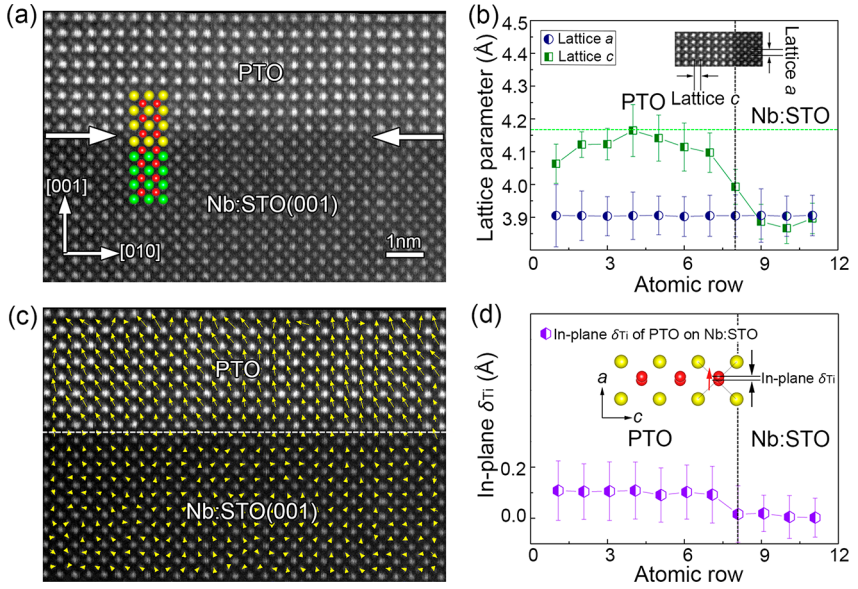

Figure 3. (a) Atomically resolved STEM image along the [100] direction of 3.2 nm thick $PbTiO_3$ on Nb:$SrTiO_3$. (b) In-plane and out-of-plane lattice parameter variations of the $PbTiO_3$ films on Nb:$SrTiO_3$ substrates. Horizontal dotted line marks the lattice parameter c of bulk tetragonal $PbTiO_3$, which is 4.157(5) Å. (c) Superposition of the reversed δ_{Ti} vectors with experimental images. The reversed δ_{Ti} vectors corresponding to $PbTiO_3$ unit cells are shown as yellow arrows superimposed on the atomic image of (a). (d) In-plane displacement of Ti^{4+} relative to Pb^{2+}, in which δ_{Ti} is defined as an inset.

images, which is shown in Figure 3c, and the in-plane δ_{Ti} is also displayed in Figure 3d. All of the results are similar to the above results where PTO is on STO.

Polarization rotation was predicted for $PbZr_{0.5}Ti_{0.5}O_3$ films under an uncompensated depolarization field,[33] which indicates that multiple polarization patterns may evolve in ferroelectric films depending on the magnitude of the depolarization field. However, the truth is that an ideally screened depolarization field may not appear in practical situations.[34] In the present study, single domain PTO films were grown on both insulating and conductive substrates. Polarization rotations were found in both PTO films, indicating that the polarization rotation does not result from depolarization fields as conductive substrates should screen depolarization fields.[35] It is worth noting that from the shift of Ti^{4+}, we find the polarization rotates to the direction that may be between [001] and [111]. The polarization rotation also means that a low symmetry phase evolves here, as also observed by Catalan *et al.*,[9] where the *ac* phase and *r* phase are both found in ultrathin PTO films under tensile strain. However, in our system, there is little or even no tensile strain. To obtain further insight, we extracted the information on the O atom.

DOI: 10.1021/acsnano.8b00862
ACS Nano 2018, 12, 3681−3688

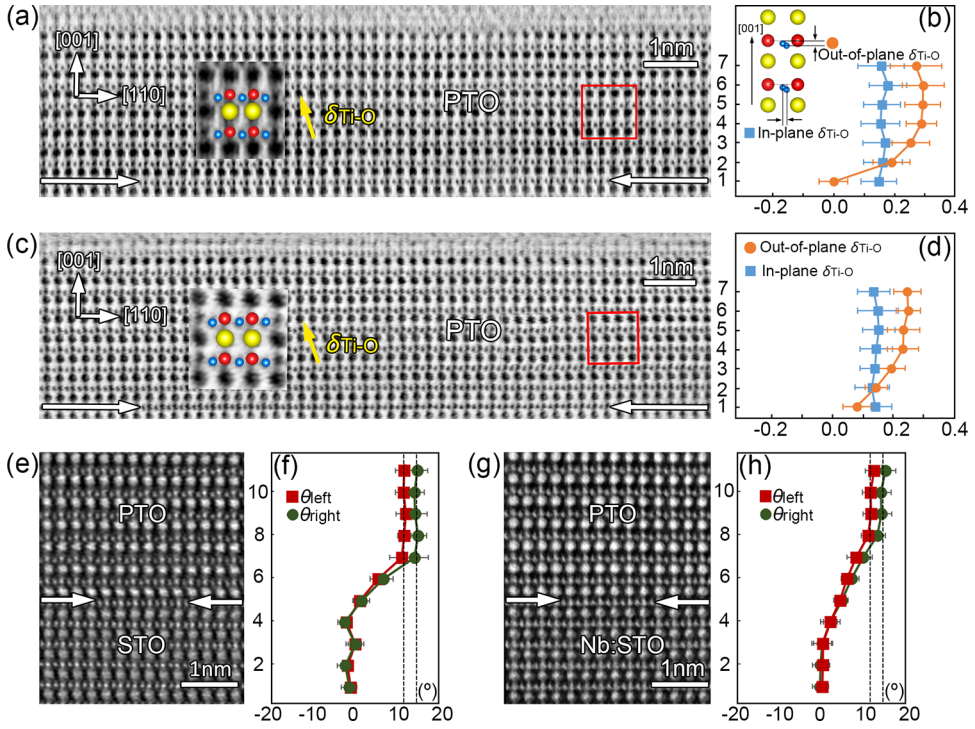

Figure 4. (a,c) ABF-STEM images along the [1$\bar{1}$0] direction of 3.2 nm thick $PbTiO_3$ films on $SrTiO_3$ and Nb:$SrTiO_3$, respectively (yellow, Pb; red, Ti; blue, O). (b,d) Quantitative results extracted from corresponding ABF images. In-plane and out-of-plane δ_{Ti-O} are defined in the inset. (e,g) ABF-STEM images along the [1$\bar{1}$0] direction of the $PbTiO_3$ films on $SrTiO_3$ and Nb:$SrTiO_3$, respectively. Contrast was inverted here to ease visual inspection. (f,h) Quantitative results show the bond angle distributions corresponding to (e,g).

The ABF-STEM imaging technique is used to record not only the Pb^{2+} and Ti^{4+} columns but also the O columns, which is powerful for imaging O atom columns. Figure 4 shows the atomic-resolution ABF-STEM images of the PTO films on STO (Figure 4a) and Nb:STO (Figure 4c). The representative areas marked by red boxes in the PTO films were magnified and are shown as insets. The relative displacements of Ti^{4+} to the center of O^{2-} octahedron (δ_{Ti-O}) are indicated by the atomic schematics in Figure 4a,c, which forms electric dipoles indicated by yellow arrows in the PTO. It is worth noting that the direction of δ_{Ti-O} is not strictly along [001] but deviates from [001]. We have extracted the magnitude of the δ_{Ti-O} distribution across the PTO film, as given in Figure 4b,d. The out-of-plane and the in-plane δ_{Ti-O} are defined in the inset in Figure 4b. The out-of-plane δ_{Ti-O} in Figure 4b,d is drastically compressed near the interface. In particular, a smaller in-plane δ_{Ti-O} was observed in both films, which indicates the signal of the O octahedra distortion. In order to gain insight into the intrinsic mechanism of this polarization rotation phenomenon, we further analyzed the ABF images. Figure 4e,g shows the inverted contrast and wiener-filtered ABF image of PTO films on STO and Nb:STO, respectively, which favors the imaging of the O atom position clearly. The bond angles are extracted and displayed in Figure 4f,h. θ_{left} and θ_{right} are defined in Figure 1c. In tetragonal PTO, the θ_{left} and θ_{right} are the same because the Ti^{4+} and oxygen octahedra are shifted only along [001]. However, in Figure 4f,h, we find the θ_{left} and θ_{right} are not equal. It is verified that the oxygen octahedra in our system different from that in tetragonal PTO. It is reported that the perovskite oxide has several types of oxygen octahedral distortion in PTO films, which may include shift and rotation[36] at the same time. In the calculated minimum energy structure, the octahedral rotation is 2° ~ 3° around [001], [110], or [111].[19,20]

From a comparison of the experiment above, we find that PTO films grown on STO or Nb:STO display polarization rotation. To gain further insight, we performed theoretical simulations for PTO films on STO.

In order to clarify the origin of the polarization rotation in ultrathin PTO films, two PTO/STO (001) models A and B were constructed, and the structural optimization was carried out based on density functional theory (DFT). The details of the calculations can be found in the Supporting Information (section 1). At the beginning, models A and B contained in-plane and out-of-plane ferroelectric (FE) polarization, that is, both in the polarization rotation state. The difference of the two models was that the oxygen octahedral rotation around the in-plane and out-of-plane axes (usually called AFD) was set to the PTO part of model B, but with no AFD in model A. In other words, a coupling of FE and AFD existed in model B, but no such coupling existed in model A. To effectively screen the depolarization field, Pb^{2+} vacancies were introduced to the surfaces of models A and B.

After full relaxation of models A and B, the corresponding schematic illustrations of polarization distributions are displayed in Figure 5a. The polarization vectors of the PTO layer in model A turn back to the [001] direction, whereas the PTO layer in model B still maintains the polarization rotation state, a phenomenon consistent with our experimental observation.

In addition, the quantitative results of the ferroelectric polarization and the rotation angle of oxygen octahedra can be obtained. In Figure 5b, the average out-of-plane polarization component P_z of the PTO layer in model A is about 77 $\mu C/cm^2$. Near the PTO/STO interface, P_z decreases gradually within about 4 unit cells. Meanwhile, the in-plane polarization component P_x in model A decreases to almost zero. In contrast, the average out-of-plane polarization component of the PTO layer in model B

DOI: 10.1021/acsnano.8b00862
ACS Nano 2018, 12, 3681−3688

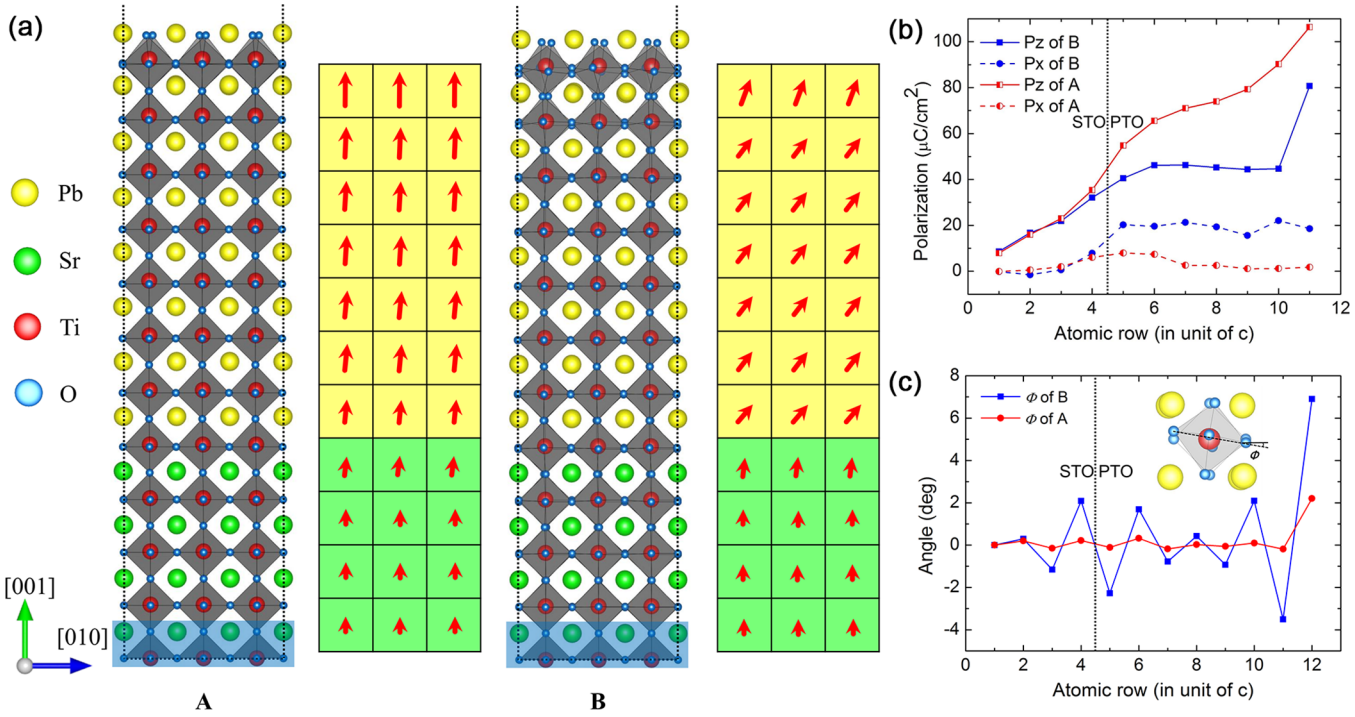

Figure 5. Results of the first-principles calculations of the ultrathin $PbTiO_3$ films grown on $SrTiO_3$ substrates. (a) Fully relaxed atomic configurations of $PbTiO_3$/ $SrTiO_3$ supercells A and B, without (left) and with (right) AFD initial distortions, respectively. The schematic illustrations of their polarization distributions are also shown. (b) In-plane and out-of-plane polarization components and (c) oxygen octahedral rotation around the in-plane and out-of-plane axes extracted from the relaxed models A and B. The interface is indicated by the black dashed line. The inset in (c) shows the oxygen octahedral rotation angle (Φ) along the in-plane axis.

is 49 $\mu C/cm^2$, smaller than that in model A, whereas the in-plane polarization components still remain (about 19 $\mu C/cm^2$), showing an impressive polarization rotation state in model B. From the distribution of the rotation angle (Φ) (Figure 5c), for model B, the unit cells near the PTO surface and the PTO/STO interface show Φ somewhat larger than those away from these two regions. For model A, the same trends still exist, but the magnitudes of Φ are much smaller. The results are consistent with previous studies showing that the FE/AFD coupling at the PTO surface and the PTO/STO interface exists,[20,22,37,38] and in-plane polarization could develop due to this coupling. In the ultrathin PTO film, the two coupling regions are very close, which would leave the whole PTO film in the AFD state and generate polarization rotations. It is expected that when the film thickness increases, the two coupling regions would not overlap with each other, and the polarization rotation state may disappear. As discussed in ref 22, the antiferrodistortion in the PTO/STO system is an interfacial effect, resulting from the combination of electrostatic and covalent effects. That is the reason why the OORs are small in both PTO and STO but large at their interfaces. Consistent with previous studies, our results reveal that AFD instability in the ultrathin PTO films and the formation of the polarization rotation state could develop due to this interfacial coupling.

In order to verify this interface coupling, we grew a series of PTO films on STO (001) with both smaller thickness (1.6 nm) and larger thicknesses (4 and 6 nm). Figure 6a–c shows the high-resolution HAADF images of these films, from which the sharp interfaces can be found. The superposition of the reversed δ_{Ti} vector mappings with the atomic images are also shown in Figure 6d–f. While the polarization in 1.6 nm film was largely suppressed, some local in-plane Ti^{4+} shifting can still be identified in Figure 6d. In 2004, Fong *et al.* found periodic

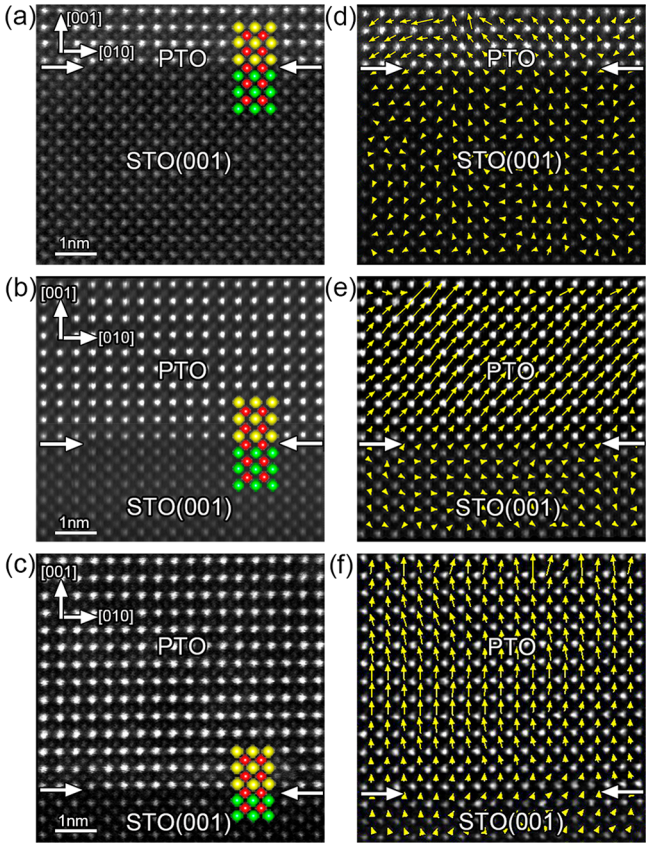

Figure 6. HAADF-STEM images of $PbTiO_3$ films on $SrTiO_3$ substrates with different thicknesses of $PbTiO_3$ for (a) 1.6 nm, (b) 4 nm, and (c) 6 nm. (d–f) Superposition of the reversed δ_{Ti} vectors with corresponding experimental images.

DOI: 10.1021/acsnano.8b00862
ACS Nano 2018, 12, 3681–3688

180° domains in PTO films down to 3 unit cells (12 Å) by synchrotron X-ray diffraction at room temperature.[39] However, in our experiment, the disordered ferroelectricity is found in ultrathin PTO films without any domain walls. We note that disordered ferroelectricity is also found in PTO/STO superlattice films, which can enhance piezoelectric response by piezoelectric force microscopy analysis.[40] In Figure 6e, the polarization rotation is found as that of Figure 3. However, this polarization rotation has vanished when the PTO film thickness is increased to 6 nm (Figure 6f), where the polarization direction of the PTO film is consistent with previous reports.[41] On the other hand, we found that the lattice parameters are suppressed in both films (Figure S1), and the suppression is weaker when the PTO layer becomes thicker. Changing trends of the lattice parameters are the same in every film as that above 3.2 nm, where lattice *a* is constant and lattice *c* decreases progressively from the film center toward the interface or the film surface.

Although strain-driven polarization rotation was established in PTO films under large tensile strains,[9] direct evidence scarcely shows such rotation in PTO films with negligible strains. Thus, the polarization rotation in PTO films observed here has confirmed the prediction by nonlinear thermodynamic phenomenological models.[42−44] Moreover, theoretical calculation has also predicted polarization rotation under different depolarization fields in PZT films.[33] In general, our results agree with these theoretical calculations. In addition, our results further indicate that interface coupling between STO and PTO is also responsible for the polarization rotation in PTO films.[45]

It is important to point out that both Ti^{4+} and the oxygen octahedron have the same displacement direction from the center of the Pb lattice even in the presence of an OOR or distortion like that in the present case. As shown in Figure 4, the δ_{Ti-O} and bond angle analyses actually reflect all the ion displacement information involving all O^{2+}, Pb^{2+}, and Ti^{4+} ions. On one hand, by combinations of Figure 2, Figure 3 (where Ti^{4+} shifts mainly downward), and Figure 4a−d (where O also shifts mainly downward relative to Ti^{4+} and Pb^{2+}), it is clear that both Ti^{4+} and the oxygen octahedron have the same displacement direction. On the other hand, there are bond angle differences between θ_{left} and θ_{right}, which indicates the rotation of oxygen octahedron. Particularly, these bond angle differences also display polarization rotation away from the *c* axis of the original tetragonal PTO unit cells, which is consistent with the Ti^{4+} ion shift maps. In fact, if there is no OOR, there will be no polarization rotation, too.

In summary, single domain $PbTiO_3$ ultrathin films on both insulating $SrTiO_3$ and conductive Nb:$SrTiO_3$ substrates with negligible strains display a polarization rotation, which is identified as a result of the interfacial oxygen octahedral coupling effect. This result is the direct experimental proof of polarization rotation in $PbTiO_3$ that was predicted by theoretical simulations. This work indicates different mechanisms and possibilities that could be used for modulating polar behaviors in ferroelectrics, tuning multiple polarization states, and piezoelectric responses of ferroelectrics.

METHODS

Materials. The $PbTiO_3$ was deposited on $SrTiO_3$ (and Nb:$SrTiO_3$) substrates by pulsed laser deposition using a Coherent ComPexPRO 201FKrF (λ = 248 nm) excimer laser. The $PbTiO_3$ targets were 3 mol % of Pb-enriched sintered ceramics. The target substrate distance was 35 mm. During the growth of $PbTiO_3$, the substrate temperature was kept at 700 °C, with a laser energy of 370 mJ, a laser repetition rate of 4 Hz, and under an oxygen pressure of 150 mTorr. Before deposition, the $SrTiO_3$ (and Nb:$SrTiO_3$) substrate was preheated at 850 °C for 10 min to clean the substrate surface and then cooled to the growth temperature (15 °C/min). The laser was focused on the ceramic target for 10 min presputtering to clean the target surface. After deposition, the film was cooled to room temperature at a cooling rate of about 5 °C/min.

STEM Sample Preparation and HAADF-STEM. Cross-sectional samples for the STEM experiments were prepared by slicing, gluing, grinding, and dimpling. A Gatan PIPS was used for the final ion milling. All STEM results were obtained using an aberration-corrected scanning transmission electron microscope (Titan Cubed 60−300 kV microscope (FEI), operated at 300 kV). This TEM is equipped with an image corrector, a probe corrector from CEOS, a high-brightness field-emission gun (X-FEG), and a monochromator. All HAADF-STEM images were recorded using a convergence semiangle of 21.4 mrad. The atom column positions were determined by fitting them as 2D Gaussian peaks using Matlab software.

First-Principles Calculations. The density functional theory calculations were performed by using a projector-augmented wave method as implemented in the VASP code. The exchange and correlation terms were considered within the local density approximation. The plane wave cutoff energy was chosen as 450 eV. The O 2s2p, Sr 4s4p5s, Ti 3s3p3d4s, and Pb 5d6s6p electrons were treated as the valence electrons. To simulate the epitaxial growth of the $PbTiO_3$ film on the $SrTiO_3$ substrate, the in-plane lattice constant of the $PbTiO_3$/$SrTiO_3$ interface model was fixed to the theoretical $SrTiO_3$ lattice constant, and the ionic relaxation was considered to be convergent when the force on every atom was less than 10 meV/Å. The lateral size of the interface model was extended to 2 × 2 to consider the OOR. The Monkhorst−Pack *k*-point meshes were chosen as 2 × 2 × 1 for the $PbTiO_3$/$SrTiO_3$ interface models. In addition, the bottom layer of $SrTiO_3$ was fixed to simulate the bulk region of the substrate, and all other layers were allowed to relax. A vacuum layer of 15 Å was added on top of the $PbTiO_3$ surface, and the dipole correction was applied to avoid spurious interactions between periodic images.

ASSOCIATED CONTENT

Supporting Information

The Supporting Information is available free of charge on the ACS Publications website at DOI: 10.1021/acsnano.8b00862.

First-principles calculations and experimental details (PDF)

AUTHOR INFORMATION

Corresponding Authors

*E-mail: ylzhu@imr.ac.cn.

*E-mail: xlma@imr.ac.cn.

ORCID

Yinlian Zhu: 0000-0002-0356-3306

Author Contributions

X.M. and Y.Z. conceived the project of interfacial characterization in oxides by using aberration-corrected STEM. S.Z., Y.Z., and X.M. designed the experiments. S.Z. performed the thin-film growth and STEM observations. Y.W., X.G., and D.C. carried out first-principles calculations. Y.T., D.M., S.L., M.H., J.M., and B.W. participated in the thin-film growth and STEM imaging. All authors contributed to the discussions and manuscript preparation.

Notes

The authors declare no competing financial interest.

ACKNOWLEDGMENTS

This work is supported by the National Natural Science Foundation of China (Nos. 51571197, 51501194, 51671194,

DOI: 10.1021/acsnano.8b00862
ACS Nano 2018, 12, 3681−3688

51401212), National Basic Research Program of China (2014CB921002), and the Key Research Program of Frontier Sciences CAS (QYZDJ-SSW-JSC010). Y.T. acknowledges the IMR SYNL-T.S. Kê Research Fellowship and the Youth Innovation Promotion Association CAS (No. 2016177). Y.W. acknowledges the support from the National Key Research Program of China (2016YFA0201001) and National Natural Science Foundation of China (No. 11627801).

REFERENCES

(1) Dawber, M.; Rabe, K. M.; Scott, J. F. Physics of Thin-Film Ferroelectric Oxides. *Rev. Mod. Phys.* **2005**, *77*, 1083−1130.
(2) Scott, J. F. Applications of Modern Ferroelectrics. *Science* **2007**, *315*, 954−959.
(3) Park, S. E.; Shrout, T. R. Ultrahigh Strain and Piezoelectric Behavior in Relaxor Based Ferroelectric Single Crystals. *J. Appl. Phys.* **1997**, *82*, 1804−1811.
(4) Fu, H. X.; Cohen, R. E. Polarization Rotation Mechanism for Ultrahigh Electromechanical Response in Single-Crystal Piezoelectrics. *Nature* **2000**, *403*, 281−283.
(5) Kvasov, A.; McGilly, L. J.; Wang, J.; Shi, Z. Y.; Sandu, C. S.; Sluka, T.; Tagantsev, A. K.; Setter, N. Piezoelectric Enhancement under Negative Pressure. *Nat. Commun.* **2016**, *7*, 12136.
(6) Li, F.; Zhang, S. J.; Yang, T. N.; Xu, Z.; Zhang, N.; Liu, G.; Wang, J. J.; Wang, J. L.; Cheng, Z. X.; Ye, Z. G.; Luo, J.; Shrout, T. R.; Chen, L. Q. The Origin of Ultrahigh Piezoelectricity in Relaxor-Ferroelectric Solid Solution Crystals. *Nat. Commun.* **2016**, *7*, 13807.
(7) Kutnjak, Z.; Petzelt, J.; Blinc, R. The Giant Electromechanical Response in Ferroelectric Relaxors as a Critical Phenomenon. *Nature* **2006**, *441*, 956−959.
(8) Liu, H.; Chen, J.; Fan, L.; Ren, Y.; Pan, Z.; Lalitha, K. V.; Rodel, J.; Xing, X. Critical Role of Monoclinic Polarization Rotation in High-Performance Perovskite Piezoelectric Materials. *Phys. Rev. Lett.* **2017**, *119*, 017601.
(9) Catalan, G.; Janssens, A.; Rispens, G.; Csiszar, S.; Seeck, O.; Rijnders, G.; Blank, D. H. A.; Noheda, B. Polar Domains in Lead Titanate Films under Tensile Strain. *Phys. Rev. Lett.* **2006**, *96*, 127602.
(10) Catalan, G.; Lubk, A.; Vlooswijk, A. H. G.; Snoeck, E.; Magen, C.; Janssens, A.; Rispens, G.; Rijnders, G.; Blank, D. H. A.; Noheda, B. Flexoelectric Rotation of Polarization in Ferroelectric Thin Films. *Nat. Mater.* **2011**, *10*, 963−967.
(11) Noheda, B.; Cox, D. E.; Shirane, G.; Gonzalo, J. A.; Cross, L. E.; Park, S. E. A Monoclinic Ferroelectric Phase in the $Pb(Zr_{1-x}Ti_x)O_3$ Solid Solution. *Appl. Phys. Lett.* **1999**, *74*, 2059−2061.
(12) Guo, R.; Cross, L. E.; Park, S. E.; Noheda, B.; Cox, D. E.; Shirane, G. Origin of the High Piezoelectric Response in $PbZr_{1-x}Ti_xO_3$. *Phys. Rev. Lett.* **2000**, *84*, 5423−5426.
(13) Kroemer, H. Nobel Lecture: Quasielectric Fields and Band Offsets: Teaching Electrons New Tricks. *Rev. Mod. Phys.* **2001**, *73*, 783−793.
(14) Reyren, N.; Thiel, S.; Caviglia, A. D.; Kourkoutis, L. F.; Hammerl, G.; Richter, C.; Schneider, C. W.; Kopp, T.; Ruetschi, A. S.; Jaccard, D.; Gabay, M.; Muller, D. A.; Triscone, J. M.; Mannhart, J. Superconducting Interfaces Between Insulating Oxides. *Science* **2007**, *317*, 1196−1199.
(15) Yin, Y. W.; Burton, J. D.; Kim, Y. M.; Borisevich, A. Y.; Pennycook, S. J.; Yang, S. M.; Noh, T. W.; Gruverman, A.; Li, X. G.; Tsymbal, E. Y.; Li, Q. Enhanced Tunnelling Electroresistance Effect Due to a Ferroelectrically Induced Phase Transition at a Magnetic Complex Oxide Interface. *Nat. Mater.* **2013**, *12*, 397−402.
(16) Liu, Y.; Zhu, Y. L.; Tang, Y. L.; Wang, Y. J.; Jiang, Y. X.; Xu, Y. B.; Zhang, B.; Ma, X. L. Local Enhancement of Polarization at $PbTiO_3/BiFeO_3$ Interfaces Mediated by Charge Transfer. *Nano Lett.* **2017**, *17*, 3619−3628.
(17) Zhang, S. R.; Zhu, Y. L.; Tang, Y. L.; Liu, Y.; Li, S.; Han, M. J.; Ma, J. Y.; Wu, B.; Chen, Z.; Saremi, S.; Ma, X. L. Giant Polarization Sustainability in Ultrathin Ferroelectric Films Stabilized by Charge Transfer. *Adv. Mater.* **2017**, *29*, 1703543.
(18) Huang, H. H.; Hong, Z.; Xin, H. L.; Su, D.; Chen, L. Q.; Huang, G.; Munroe, P. R.; Valanoor, N. Nanoscale Origins of Ferroelastic Domain Wall Mobility in Ferroelectric Multilayers. *ACS Nano* **2016**, *10*, 10126−10134.
(19) Blok, J. L.; Blank, D. H. A.; Rijnders, G.; Rabe, K. M.; Vanderbilt, D. Interplay of Epitaxial Strain and Rotations in $PbTiO_3/PbZrO_3$ Superlattices From First Principles. *Phys. Rev. B: Condens. Matter Mater. Phys.* **2011**, *84*, 205413.
(20) Bousquet, E.; Dawber, M.; Stucki, N.; Lichtensteiger, C.; Hermet, P.; Gariglio, S.; Triscone, J. M.; Ghosez, P. Improper Ferroelectricity in Perovskite Oxide Artificial Superlattices. *Nature* **2008**, *452*, 732−736.
(21) Li, M.; Li, J.; Chen, L. Q.; Gu, B. L.; Duan, W. Effects of Strain and Oxygen Vacancies on the Ferroelectric and Antiferrodistortive Distortions in $PbTiO_3/SrTiO_3$ Superlattice. *Phys. Rev. B: Condens. Matter Mater. Phys.* **2015**, *92*, 115435.
(22) Aguado-Puente, P.; Garcia-Fernandez, P.; Junquera, J. Interplay of Couplings between Antiferrodistortive, Ferroelectric, and Strain Degrees of Freedom in Monodomain $PbTiO_3/SrTiO_3$ Superlattices. *Phys. Rev. Lett.* **2011**, *107*, 217601.
(23) Kim, T. H.; Puggioni, D.; Yuan, Y.; Xie, L.; Zhou, H.; Campbell, N.; Ryan, P. J.; Choi, Y.; Kim, J. W.; Patzner, J. R.; Ryu, S.; Podkaminer, J. P.; Irwin, J.; Ma, Y.; Fennie, C. J.; Rzchowski, M. S.; Pan, X. Q.; Gopalan, V.; Rondinelli, J. M.; Eom, C. B. Polar Metals by Geometric Design. *Nature* **2016**, *533*, 68−72.
(24) Rondinelli, J. M.; Spaldin, N. A. Substrate Coherency Driven Octahedral Rotations in Perovskite Oxide Films. *Phys. Rev. B: Condens. Matter Mater. Phys.* **2010**, *82*, 113402.
(25) Liao, Z.; Huijben, M.; Zhong, Z.; Gauquelin, N.; Macke, S.; Green, R. J.; Van Aert, S.; Verbeeck, J.; Van Tendeloo, G.; Held, K.; Sawatzky, G. A.; Koster, G.; Rijnders, G. Controlled Lateral Anisotropy in Correlated Manganite Heterostructures by Interface-Engineered Oxygen Octahedral Coupling. *Nat. Mater.* **2016**, *15*, 425−431.
(26) Kuroiwa, Y.; Aoyagi, S.; Sawada, A.; Harada, J.; Nishibori, E.; Takata, M.; Sakata, M. Evidence for Pb-O Covalency in Tetragonal $PbTiO_3$. *Phys. Rev. Lett.* **2001**, *87*, 217601.
(27) Tang, Y. L.; Zhu, Y. L.; Ma, X. L.; Borisevich, A. Y.; Morozovska, A. N.; Eliseev, E. A.; Wang, W. Y.; Wang, Y. J.; Xu, Y. B.; Zhang, Z. D.; Pennycook, S. J. Observation of a Periodic Array of Flux-Closure Quadrants in Strained Ferroelectric $PbTiO_3$ Films. *Science* **2015**, *348*, 547−551.
(28) Pennycook, S. J.; Boatner, L. A. Chemically Sensitive Structrure Imaging with a Scanning Transmission Electron Microscope. *Nature* **1988**, *336*, 565−567.
(29) Jia, C. L.; Nagarajan, V.; He, J. Q.; Houben, L.; Zhao, T.; Ramesh, R.; Urban, K.; Waser, R. Unit-Cell Scale Mapping of Ferroelectricity and Tetragonality in Epitaxial Ultrathin Ferroelectric Films. *Nat. Mater.* **2007**, *6*, 64−69.
(30) Gao, P.; Zhang, Z. Y.; Li, M. Q.; Ishikawa, R.; Feng, B.; Liu, H. J.; Huang, Y. L.; Shibata, N. S.; Ma, X. M.; Chen, S. L.; Zhang, J. M.; Liu, K. H.; Wang, E. G.; Yu, D. P.; Liao, L.; Chu, Y. H.; Ikuhara, Y. Possible Absence of Critical Thickness and Size Effect in Ultrathin Perovskite Ferroelectric Films. *Nat. Commun.* **2017**, *8*, 15549.
(31) Anthony, S. M.; Granick, S. Image Analysis with Rapid and Accurate Two-Dimensional Gaussian Fitting. *Langmuir* **2009**, *25*, 8152−8160.
(32) Wang, W. Y.; Zhu, Y. L.; Tang, Y. L.; Xu, Y. B.; Liu, Y.; Li, S.; Zhang, S. R.; Wang, Y. J.; Ma, X. L. Large Scale Arrays of Four-State Vortex Domains in $BiFeO_3$ Thin Film. *Appl. Phys. Lett.* **2016**, *109*, 202904.
(33) Kornev, I.; Fu, H. X.; Bellaiche, L. Ultrathin Films of Ferroelectric Solid Solutions Under a Residual Depolarizing Field. *Phys. Rev. Lett.* **2004**, *93*, 196104.
(34) Mehta, R. R.; Silverman, B. D.; Jacobs, J. T. Depolarization Fields in Thin Ferroelectric Films. *J. Appl. Phys.* **1973**, *44*, 3379−3385.
(35) Lichtensteiger, C.; Triscone, J. M.; Junquera, J.; Ghosez, P. Ferroelectricity and Tetragonality in Ultrathin $PbTiO_3$ Films. *Phys. Rev. Lett.* **2005**, *94*, 047603.

DOI: 10.1021/acsnano.8b00862
ACS Nano 2018, 12, 3681−3688

(36) Glazer, A. M. Simple Ways of Determining Perovskite Structures. *Acta Crystallogr., Sect. A: Cryst. Phys., Diffr., Theor. Gen. Crystallogr.* **1975**, *31*, 756−762.
(37) Munkholm, A.; Streiffer, S. K.; Ramana Murty, M. V.; Eastman, J. A.; Thompson, C.; Auciello, O.; Thompson, L.; Moore, J. F.; Stephenson, G. B. Antiferrodistortive Reconstruction of the $PbTiO_3$(001) Surface. *Phys. Rev. Lett.* **2001**, *88*, 016101.
(38) Bungaro, C.; Rabe, K. M. Coexistence of Antiferrodistortive and Ferroelectric Distortions at the $PbTiO_3$(001) Surface. *Phys. Rev. B: Condens. Matter Mater. Phys.* **2005**, *71*, 035420.
(39) Fong, D. D.; Stephenson, G. B.; Streiffer, S. K.; Eastman, J. A.; Auciello, O.; Fuoss, P. H.; Thompson, C. Ferroelectricity in Ultrathin Perovskite Films. *Science* **2004**, *304*, 1650−1653.
(40) Kim, G. Y.; Chu, K.; Sung, K. D.; Lee, H. S.; Kim, S. D.; Song, K.; Choi, T.; Lee, J.; Buban, J. P.; Yoon, S. Y.; Kim, K. H.; Yang, C. H.; Choi, S. Y. Disordered Ferroelectricity in the $PbTiO_3/SrTiO_3$ Superlattice Thin Film. *APL Mater.* **2017**, *5*, 066104.
(41) Despont, L.; Koitzsch, C.; Clerc, F.; Garnier, M. G.; Aebi, P.; Lichtensteiger, C.; Triscone, J. M.; Garcia de Abajo, F. J.; Bousquet, E.; Ghosez, P. Direct Evidence for Ferroelectric Polar Distortion in Ultrathin Lead Titanate Perovskite Films. *Phys. Rev. B: Condens. Matter Mater. Phys.* **2006**, *73*, 094110.
(42) Pertsev, N. A.; Zembilgotov, A. G.; Tagantsev, A. K. Effect of Mechanical Boundary Conditions on Phase Diagrams of Epitaxial Ferroelectric Thin Films. *Phys. Rev. Lett.* **1998**, *80*, 1988−1991.
(43) Qiu, Q. Y.; Nagarajan, V.; Alpay, S. P. Film Thickness *versus* Misfit Strain Phase Diagrams for Epitaxial $PbTiO_3$ Ultrathin Ferroelectric Films. *Phys. Rev. B: Condens. Matter Mater. Phys.* **2008**, *78*, 064117.
(44) Ma, W. Polarization Rotation Associated Critical Phenomena in Epitaxial $PbTiO_3$ Thin Films Near Room Temperature. *AIP Adv.* **2016**, *6*, 045310.
(45) Xue, Y. B.; Chen, D.; Wang, Y. J.; Tang, Y. L.; Zhu, Y. L.; Ma, X. L. The Evolution of Polarization inside Ultrathin $PbTiO_3$ Films: a Theoretical Study. *Philos. Mag.* **2015**, *95*, 2067−2077.

DOI: 10.1021/acsnano.8b00862
ACS Nano 2018, 12, 3681−3688